

# A new model for the metal–support interaction Evidence for a shift in the energy of the valence orbitals

J.T. Miller<sup>a,\*</sup>, B.L. Mojet<sup>b,1</sup>, D.E. Ramaker<sup>c</sup>, D.C. Koningsberger<sup>b</sup>

<sup>a</sup> BP Amoco Chemicals Research Center, Mail Station E-1F, 150 West Warrenville Road, Naperville, IL 60563-8460, USA

<sup>b</sup> Debye Institute, Department of Inorganic Chemistry, Utrecht University, PO Box 80083, 3508 TB Utrecht, Netherlands

<sup>c</sup> Chemistry Department, George Washington University, Washington, DC 20052, USA

## Abstract

The catalytic and spectroscopic properties of Pt supported on LTL zeolite are greatly affected by the acidity/alkalinity of the support. The turnover frequency (TOF) for neopentane hydrogenolysis and isomerization decreases from acidic to neutral to alkaline. In addition, in the infrared spectra, there is a decrease in the linear to bridging ratio of adsorbed CO which parallels the catalytic activity, indicating that the changes in TOF are due to a modification of the electronic properties of the Pt particles resulting from the metal–support interaction. The local structure of the Pt particles has also been determined by EXAFS spectroscopy. The Pt atoms are in contact with the oxygen ions of the support. None of the Al, Si or K ions are within bonding distance of the Pt. In addition, analysis of the L<sub>III</sub> and L<sub>II</sub> near-edge spectra suggest that, contrary to the generally accepted model, the number of electrons in the valence band is unchanged by the support interaction. Furthermore, at the L<sub>III</sub> edge in the presence of chemisorbed hydrogen, a Pt–H antibonding orbital is observed near the Fermi level. Isolation of this shape resonance indicates that the energy difference between the antibonding orbital and the Fermi level increases with increasing acidity of the support and correlates with the TOF. Based on the analysis of the Pt–H shape resonance, a new model for the metal–support interaction is proposed where the binding energy of the Pt valence orbitals increase as the charge of the support oxide ion becomes more positive, i.e., becomes more acidic. The catalytic and spectroscopic properties are discussed in the context of this new model. © 2000 Elsevier Science B.V. All rights reserved.

**Keywords:** Metal–support interaction; Shape resonance; Pt XANES; Pt EXAFS; Pt/LTL catalysts; Neopentane hydrogenolysis; Infrared spectra of CO on Pt

## 1. Introduction

Supported noble metal catalysts are used in a large number of commercially important processes, including hydrogenation, naphtha reforming, oxidation, au-

tomotive exhaust catalysts and fuel cells. It is known that the support influences the catalytic properties of noble metal particles, resulting in an increase in the turnover frequency (TOF) on acidic supports [1–11] and a decrease on alkaline supports [9–11]. Further, metal particles on acidic supports are more sulfur resistant [12–20]. These changes in catalytic properties are generally ascribed to a modification of the electronic properties of the metal particles resulting from a metal–support interaction [1–6,9–11,21]. Shifts in the stretching frequency [9,11,22,23] and a change from linear to bridge bonding of adsorbed CO [9,11]

\* Corresponding author. Tel.: +1-630-420-5818;  
fax: +1-630-420-3636.

E-mail address: millejt1@bp.com (J.T. Miller).

<sup>1</sup> Present address: Schuit Institute of Catalysis, Eindhoven University of Technology, PO Box 513, 5600 MB Eindhoven, Netherlands.

suggest that metals are electron deficient on acidic supports and electron rich on alkaline supports. Similarly, shifts in the binding energy in the photoelectron spectra [6,9,24] are consistent with the proposal that acidic supports withdraw electron density from the metal, while alkaline supports donate electron density to the metal. The general interpretation for the metal–support interaction, therefore, is that changes in catalytic and spectroscopic properties result from a change in the number of electrons in the valence orbitals.

Several electronic models for the metal–support interaction have previously been proposed. Based on a correlation of the TOF with the calculated charge on the oxide ions of the support [4], one model proposes that there is a partial electron transfer between the metal and the oxygen [4,9,11]. Acidic supports are thought to withdraw electron density resulting in electron deficient metal particles. An alternative model proposes that support protons interact with the metal particles forming metal–proton adducts [5,6]. The proton is delocalized over the metal particle and withdraws electron density from the surface atoms. As in the previous model, the increase in TOF on acidic supports is due to electron deficient metal particles. These two models are similar in that they both propose that there is a transfer of electron density due to the metal–support interaction. The difference in the models is that in the former the transfer is thought to occur between the metal and the oxide ions, while in the latter the metal transfers electron density to the support protons. Finally, a third model based on theoretical calculations proposes that in small metal clusters highly charged cations of the support attract electrons of nearby metal atoms [25,26]. As a result, the electron density of the atoms near the support surface increases, while the atoms on the opposite side of the cluster, i.e., those that participate in the catalysis, are electron deficient. In this model, there is no net change in electron density of the cluster; however, polarization of the electron density leaves those atoms which participate in the catalysis electron deficient.

In this paper, the TOFs and infrared spectra of adsorbed CO have been determined for a series of Pt/LTL zeolite catalysts with differing acidity/alkalinity. The local structure of the Pt particles has also been determined by EXAFS spectroscopy. Moreover, a new analysis of the  $L_{III}$  and  $L_{II}$  near-edge spectra is presented. Changes in the valence band

contribution to the near-edge spectra are small and do not correlate with the changes in the support composition, TOF or infrared spectra. In the presence of chemisorbed hydrogen, at the  $L_{III}$  edge a Pt–H antibonding orbital is observed near the Fermi level. Isolation of this shape resonance indicates that the energy difference between the antibonding orbital and Fermi level is affected by the acidity/alkalinity of the support. Based on the near edge analysis, a new model for the metal–support interaction is proposed where the change in the charge density of the support oxide ions induces a shift in the energy of the Pt valence orbitals, rather than a change in the number of valence electrons. The catalytic and spectroscopic properties are discussed in the context of this new model.

## 2. Experimental

### 2.1. Catalyst preparation

The acidity/alkalinity of the LTL zeolite supports was varied by impregnating a commercial K-LTL zeolite (from UOP) with  $KNO_3$ , or exchanging with  $NH_4NO_3$ , to give K/Al ratios ranging from 0.63 to 1.45. Each LTL zeolite was calcined at 225°C. Platinum was added by incipient wetness impregnation using an aqueous solution of  $[Pt(NH_3)_4](NO_3)_2$ , followed by drying at 125°C. The catalysts are designated by Pt/LTL ( $x$ ) with  $x$  representing the K/Al molar ratio. The elemental analysis and platinum dispersion determined by  $H_2$  chemisorption are given in Table 1.

### 2.2. Neopentane hydrogenolysis

Catalytic activities and selectivities were determined in a 1.25 cm ID, quartz, plug-flow microreactor at atmospheric pressure. An internal thermocouple was positioned in the center of the catalyst bed, and the reaction temperature was 350°C. The gas composition was 0.99% neopentane in hydrogen, and the flow rate was controlled by Brooks 5872 mass flow controller. Catalyst loadings between 0.1 and 0.5 g (100 mesh and diluted with 2 cm<sup>3</sup> of  $\alpha$ -alumina) were pre-reduced in flowing hydrogen at the reaction temperature for 1 h. The flow rate was adjusted to keep the conversion below 5%, and the outlet composition

Table 1  
Elemental analysis, Pt dispersion and neopentane conversion

Pt/LTL catalyst <sup>a</sup>	Al (wt.%)	K (wt.%)	Dispersion <sup>b</sup>	TOF <sup>c</sup>	Hydrogenolysis selectivity
LTL (0.63)	9.1	8.3	0.53	$2.2 \times 10^{-1}$	0.89
LTL (0.83)	8.5	10.2	0.81	$1.9 \times 10^{-1}$	0.80
LTL (0.93)	8.6	11.6	0.86	$1.0 \times 10^{-1}$	0.84
LTL (0.96)	8.5	11.8	0.89	$4.8 \times 10^{-2}$	0.77
LTL (1.16)	9.1	15.3	1.14	$2.5 \times 10^{-3}$	0.71
LTL (1.25)	8.8	15.9	0.88	$7.2 \times 10^{-5}$	0.68
LTL (1.45)	8.6	18.1	0.43	$6.0 \times 10^{-6}$	ND

<sup>a</sup> Values in brackets represent K/Al molar ratio.

<sup>b</sup> Determined by volumetric H<sub>2</sub> chemisorption assuming one H/Pt atom.

<sup>c</sup> Molecules per secondary surface Pt atom, TOF of Pt/LTL (1.45) was determined at 475°C and estimated at 350°C by comparison with Pt/LTL (1.25).

was analyzed by gas chromatography equipped with an FID detector. The selectivity was calculated on a molar basis as the fraction of neopentane converted to isopentane (isomerization), or methane plus isobutane (hydrogenolysis). The TOFs and hydrogenolysis selectivities are also given in Table 1. Control experiments with  $\alpha$ -alumina showed no measurable conversion.

### 2.3. Infrared spectroscopy

Transmission infrared spectra were recorded on a Perkin-Elmer 1720-X Fourier Transform spectrometer with a spectral resolution of 4 cm<sup>-1</sup>. The catalysts were pressed into thin self-supporting wafers and placed in an in situ transmission infrared cell. The catalyst was reduced in H<sub>2</sub> at 300°C and cooled to room temperature. Subsequently, the sample was purged with He for 10 min followed by flowing 20% CO in He gas for 10 min, after which the CO absorbance spectrum was collected. The spectra were corrected for the absorption of the support and gas phase CO.

### 2.4. X-ray absorption spectroscopy

The X-ray absorption spectra of Pt at the L<sub>III</sub> and L<sub>II</sub> edges were taken at Daresbury Wiggler Station 9.2, using a Si (2 2 0) double crystal monochromator. The measurements were done in transmission mode using ion chambers filled with Ar to have a  $\mu x$  of 20% in the first and a  $\mu x$  of 80% in the second ion chamber. The monochromator was detuned to 50% maximum inten-

sity at 12 250 eV to avoid higher harmonics present in the X-ray beam.

Samples were pressed into a self-supporting wafer (calculated to have an absorbance of 2.5) and placed in a controlled atmosphere cell. The catalysts were reduced in flowing hydrogen at 300°C (flow: 100 cm<sup>3</sup> min<sup>-1</sup>, ramp: 5°C min<sup>-1</sup>, hold: 1 h), and measured under a hydrogen atmosphere at liquid nitrogen temperature. Samples measured in the presence of chemisorbed hydrogen are designated (H<sub>2</sub>) Pt/LTL. Additionally, chemisorbed hydrogen was desorbed from the reduced catalyst at 300°C for 1 h in flowing He. Spectra were taken at liquid nitrogen temperature under continuous evacuation. These samples are designated Pt/LTL.

### 2.5. EXAFS data analysis

Standard procedures were used to extract the EXAFS data from the measured absorption spectra. The pre-edge background was approximated by a modified Victoreen curve, and the background was subtracted using cubic spline routines [27]. The data were normalized by dividing by the height of the absorption edge. The EXAFS data were fit in *R*-space using the commercially available data analysis package XDAP [28]. The fits were optimized by application of the difference file technique with phase and amplitude corrected Fourier transforms [29,30]. The EXAFS data for the Pt/LTL catalysts were fit using Pt–Pt and Pt–O phase functions and backscattering amplitudes calculated with the FEFF7 code. The theoretical references were calibrated with the experimental EXAFS data for

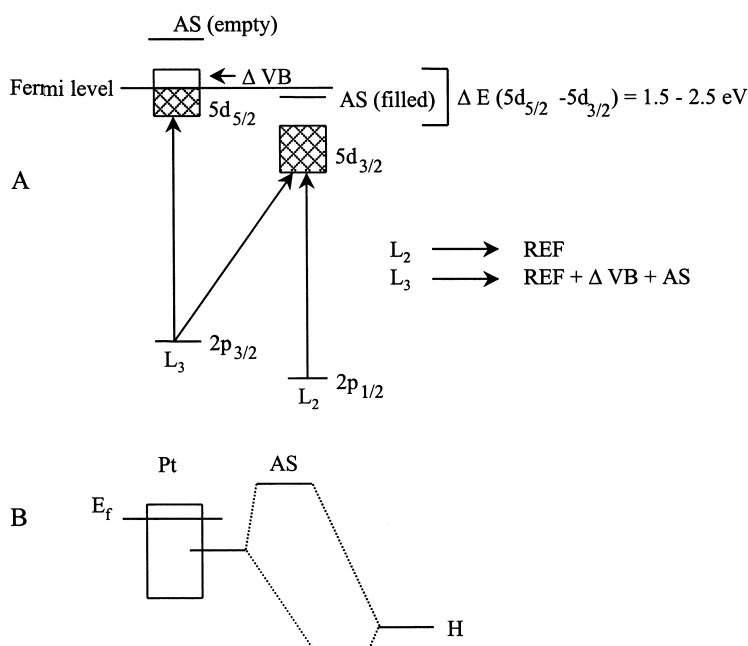


Fig. 1. (A) Contributions to the Pt  $L_{III}$  and  $L_{II}$  near-edge X-ray adsorption spectra, including the allowed transitions, the effect of spin-orbit coupling and chemisorbed hydrogen. (B) Illustration of the bonding and antibonding (AS) molecular orbitals of Pt valence orbitals with H 1s orbital.

Pt-foil and  $\text{Na}_2\text{Pt}(\text{OH})_6$ . The errors in the calculated parameters were 5% in coordination number  $N$ , 1% in distance  $R$ , 5% in Debye Waller factor  $\Delta\sigma^2$ , and 10% in the inner potential shift  $\Delta E_0$ .

### 2.6. Theoretical analysis of the Pt $L_{III}$ and $L_{II}$ near-edge X-ray absorption spectra

Analysis of the  $L_{II}$  and  $L_{III}$  near-edge absorption spectra is based upon the theoretical concepts which are schematically shown in Fig. 1 [31]. The spin-orbit interaction in both the core and valence levels introduces large differences between the  $L_{III}$  ( $2p_{3/2} \rightarrow 5d_{5/2}, 5d_{3/2}$ ) and  $L_{II}$  ( $2p_{1/2} \rightarrow 5d_{3/2}$ ) edges both in shape and intensity [32]. The  $2p_{3/2}-2p_{1/2}$  splitting is around 1709 eV and the  $5d_{5/2}-5d_{3/2}$  splitting is around 1.5–2.5 eV. The  $L_{III}$  edge reflects the empty valence levels ( $\Delta VB$ ) of both the  $d_{5/2}$  and  $d_{3/2}$  bands, weighted as  $d_{5/2}/d_{3/2} = 6$ ; however, the  $L_{II}$  edge reflects only the  $d_{3/2}$  level. For small platinum clusters, the  $5d_{3/2}$  band is believed to be completely filled due to band narrowing relative to bulk platinum; therefore,

there is no Pt d valence band ( $\Delta VB$ ) contribution at the  $L_{II}$  edge.

Hydrogen chemisorption induces a bonding and antibonding orbital [33]. As illustrated in Fig. 1B, the Pt–H bonding orbital is primarily localized on the H atom and the antibonding state (AS) is localized on the surface Pt atoms. The energy of the AS has been calculated to be approximately 1 eV higher in energy than that of the valence band. Therefore, the AS at the  $L_{III}$  absorption edge is above the Fermi level and will be observed in the near-edge spectrum, while at the  $L_{II}$  absorption edge the AS is below the Fermi level and will not be observed.

The antibonding orbital can be viewed as a localized state degenerate with the continuum, here described by the Pt–H EXAFS final-state wave function. At the  $L_{III}$  edge, the outgoing electron will reside temporarily in the potential well determined by the AS state and can escape, undergoing a resonance with the Pt–H EXAFS final-state wave function. This one-electron process causes a shape resonance with a Fano resonance line shape [34]. Its effect on the scattering cross section,  $\sigma(E)$ , can be related to an EXAFS function,  $\chi(E)$ ,

Table 2  
Contributions to the Pt L<sub>III</sub> and L<sub>II</sub> near-edge X-ray absorption spectra

Sample	L <sub>III</sub> edge	L <sub>II</sub> edge
(H <sub>2</sub> ) Pt	REF + ΔXAFS + ΔVB + AS	REF + ΔXAFS
Pt	REF + ΔVB	REF

via the normal expression,  $\sigma(E) = \mu(E)(1 + \chi(E))$ . It can be shown that

$$\chi(E) = A \sin \Phi \left[ \frac{1 - q\varepsilon}{1 + \varepsilon^2} \right]$$

where  $A$  is the amplitude factor,  $q = \cot \Phi$  and  $\varepsilon = (E - E_{\text{res}})/\Gamma$ .  $\Phi$  can be related to the usual total phase found in EXAFS containing the  $2kr$  term and the phase from the absorbing and backscattering atoms;  $\varepsilon$  is the normalized energy scale relative to the resonance energy ( $E_{\text{res}}$ ), and  $\Gamma$  represents the resonance width. A fit to the experimentally observed AS line shape gives values for  $E_{\text{res}}$ ,  $\Gamma$ ,  $A$  and  $\Phi$ .

Table 2 summarizes the contributions to the four X-ray absorption edges in the Pt/LTL catalysts with and without chemisorbed hydrogen. The L<sub>II</sub> edge spectrum for the Pt clusters without chemisorbed hydrogen will be used as the reference (REF) since this spectrum arises from the “free” atom absorption and the EXAFS contributions. The L<sub>III</sub> spectrum of Pt without chemisorbed hydrogen also contains an electronic contribution due to the partially filled valence band ( $\Delta\text{VB}$ ). In the presence of chemisorbed hydrogen, there are changes in the XAFS scattering ( $\Delta\text{XAFS}$ ) resulting from geometric changes in the Pt–Pt distance and scattering from hydrogen atoms. Finally, the L<sub>III</sub> spectrum of Pt with chemisorbed hydrogen contains contributions to the scattering from the geometric ( $\Delta\text{XAFS}$ ) and electronic ( $\Delta\text{VB}$ ) changes plus the antibonding Pt–H state (AS).

Before the different contributions ( $\Delta\text{VB}$ ,  $\Delta\text{XAFS}$ , AS) can be separated from the X-ray absorption spectra, the edges have to be aligned in order to account for initial and final state effects. The small differences in normal EXAFS contributions are negligible at the onset of the L<sub>II</sub> X-ray absorption edge. Therefore, the L<sub>II</sub> edges of Pt/LTL with and without chemisorbed hydrogen have the same shape at the onset. This allows the L<sub>II</sub> edges to be aligned in order to remove any initial state core level shifts due to the chemisorption of

hydrogen (observed to be 0.2–0.3 eV in the raw data). In practice, the L<sub>II</sub> edges were aligned where the step height was 0.6. Since both L<sub>III</sub> edges contain different electronic contributions ( $\Delta\text{VB}$  and/or AS), they have different onsets. Final-state effects determine these onsets. The L<sub>III</sub> and L<sub>II</sub> spectra of the same sample have the same EXAFS oscillations, however, which can be used for alignment of the L<sub>III</sub> edge relative to the L<sub>II</sub> edge. Thus, all edges are aligned relative to the reference, i.e., L<sub>II</sub> without chemisorbed hydrogen.

### 3. Results

#### 3.1. Neopentane hydrogenolysis

The reaction products for neopentane conversions between 0.5 and 5.0% were analyzed by the Delplot method [35] and indicate that methane, isobutane (hydrogenolysis) and isopentane (isomerization) are primary products typical of mono-functional, metal-catalyzed reactions. Methane and isobutane are produced in nearly equimolar amounts. The hydrogenolysis selectivities are given in Table 1. At 350°C, the hydrogenolysis selectivity of all catalysts is greater than 0.7 and, generally, increases with increasing support acidity.

The TOF for neopentane conversion is also given in Table 1. The TOF increases as the composition of the support changes from alkaline to neutral to acidic. Compared to neutral LTL (0.96), increasing the alkali level results in a large decrease in the TOF, while increasing number of support protons results in a smaller increase in the TOF. For example, after exchange of 30% of the K ions with protons, the TOF of Pt/LTL (0.63) is about four times greater than that of Pt/LTL (0.96). By contrast, following a 30% increase in the number of K<sup>+</sup> ions, the TOF of Pt/LTL (1.25) is more than 600 times lower than that of Pt/LTL (0.96). The TOF increases by about  $3 \times 10^4$  as the support composition changes from highly alkaline to highly acidic.

#### 3.2. Infrared spectroscopy

The Fourier transform infrared spectra of the Pt/LTL (0.63), Pt/LTL (0.93) and Pt/LTL (1.25) catalysts are displayed in Fig. 2 and are typical for supported

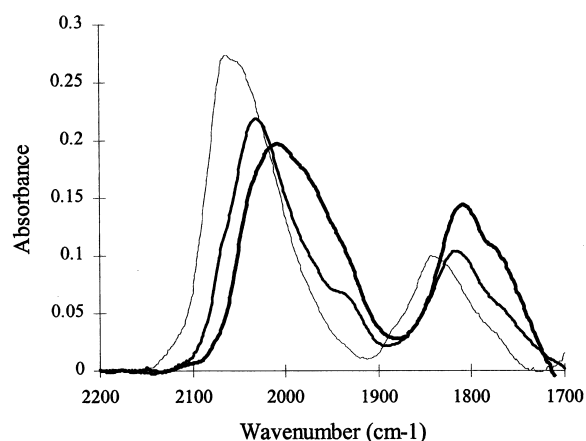


Fig. 2. Transmission FT-IR spectra of CO adsorbed on Pt/LTL catalysts: (thin) Pt/LTL (0.63); (medium) Pt/LTL (0.96); (bold) Pt/LTL (1.25).

Pt. Two regions can be assigned: linearly adsorbed CO at higher wave number and bridge-bonded CO at lower wave number. Both adsorption bands shift to lower wave number as the support composition changes from acidic to neutral to alkaline. Shifts in the CO stretching frequency are generally interpreted as evidence of changes in the electronic properties of supported metals [22,23]. The exact frequency of the absorption bands, however, depends on particle size [36], surface coverage [37] and electronic changes in

the metal structure. Since the bands are broad and the particle size is not exactly the same, the frequency shifts are not a reliable indication of a change in electronic properties.

Theoretical calculations have shown that the ratio of bridge-bonded CO increases at the expense of linear bonding when the binding energy of the metal electrons is located closer, i.e., at lower binding energy, to the energy of the CO  $2\pi^*$  orbital [38]. As the binding energy of the metal orbital decreases, there is a better overlap between the d and  $\pi^*$  orbitals, resulting in a back donation towards CO. The integrated intensity ratio of linear/bridge-bonded CO, therefore, is a direct measure of the overlap of the metal valence orbitals with the CO  $\pi^*$  orbitals. As shown in Fig. 2, there is a shift from linear to bridge-bonded CO as the alkalinity of the support increases. The infrared spectra indicate that there are changes in the electronic properties of the metal particle due to a metal–support interaction.

### 3.3. EXAFS structural analysis

The details of the XAFS analysis are given elsewhere [39]. A summary of the EXAFS parameters is given in Table 3. The metal particles in the Pt/LTL catalysts are very small with first shell Pt–Pt coordination numbers less than about 4, i.e., the average metal particle consists of approximately six atoms. The Pt–Pt

Table 3

Fit parameters of (H<sub>2</sub>) Pt/LTL and Pt/LTL EXAFS spectra ( $\Delta k = 3.2\text{--}14 \text{ \AA}^{-1}$ ;  $\Delta R = 1.8\text{--}3.1 \text{ \AA}^{-1}$ )

Catalyst	Scatterer	<i>N</i>	<i>R</i> (Å)	$\Delta\sigma^2$ ( $10^{-3} \text{ \AA}^2$ )	$\Delta E_0$ (eV)
(H <sub>2</sub> ) Pt/LTL (0.63)	Pt	3.7	2.74	4.6	−2.2
	O	2.1	2.69	4.8	7.3
(H <sub>2</sub> ) Pt/LTL (0.96)	Pt	4.2	2.74	3.5	−1.5
	O	1.6	2.69	0.9	4.5
(H <sub>2</sub> ) Pt/LTL (1.25) <sup>a</sup>	Pt	2.3	2.72	3.3	9.3
	O	3.0	2.64	10.5	5.6
Pt/LTL (0.63)	Pt	4.2	2.72	4.4	3.1
	O	1.0	2.56	2.4	10.6
	O	0.3	2.26	−6.0	−2.1
Pt/LTL (0.96)	Pt	4.3	2.71	4.2	3.4
	O	1.1	2.58	−1.4	11.8
Pt/LTL (1.25)	Pt	2.0	2.70	2.0	6.3
	O	1.3	2.61	−1.1	5.6

<sup>a</sup>  $\Delta k = 3.2\text{--}11.0 \text{ \AA}^{-1}$ , due to low signal to noise ratio as only one spectrum was available.

distance of 2.7 Å is characteristic of metallic Pt. The Pt–O distance of approximately 2.68 Å is longer than the sum of the atomic radii and has previously been attributed to the presence of hydrogen between the metal particle and the support. No potassium, silicon or aluminum ions were detected near the platinum particles in any sample. Loss of chemisorbed hydrogen resulted in very small differences in these coordination numbers and distances.

### 3.4. Analysis of the near-edge absorption spectra

Fig. 3 displays the  $L_{III}$  and  $L_{II}$  X-ray absorption edges in the presence and absence of chemisorbed hydrogen for Pt/LTL (0.96). As previously observed, the intensity of the white line is larger in the presence of chemisorbed hydrogen [40–43]. In addition, in the presence of chemisorbed hydrogen, the onset of the  $L_{III}$  edge is shifted to higher energy by about 1 eV. The near-edge spectra of the other catalysts (not shown) are similar.

Isolation of the electronic and geometric contributions to the near-edge spectra can be determined by

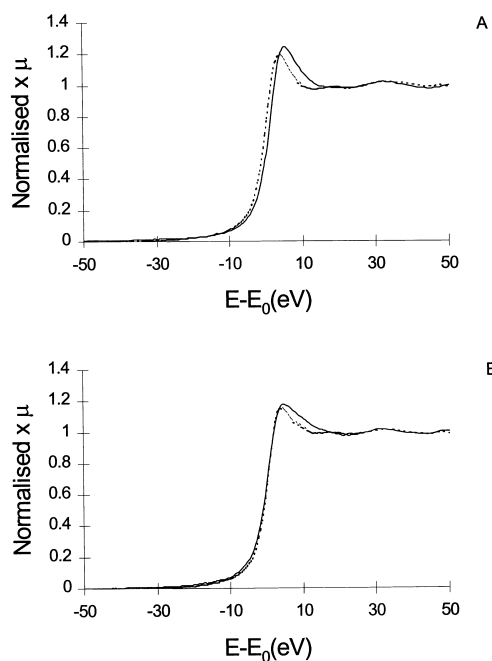


Fig. 3. Pt X-ray absorption edge with (dotted line) and without (solid line) chemisorbed hydrogen. (A)  $L_{III}$  and (B)  $L_{II}$ .

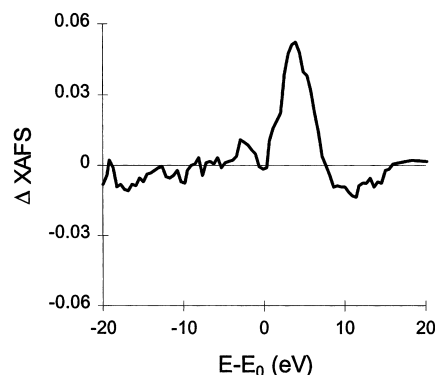


Fig. 4.  $\Delta L_{II} = L_{II}(H_2-Pt) - L_{II}(Pt) = \Delta XAFS$  for Pt/LTL (1.25).

subtracting the different edges. The geometric contributions to the near-edge spectra are determined by subtracting the  $L_{II}$  edges with and without chemisorbed hydrogen:  $\Delta L_{II} = L_{II}(H_2-Pt) - L_{II}(Pt) = \Delta XAFS$ . Fig. 4, e.g., shows  $\Delta XAFS$  for Pt/LTL (1.25). Previously, comparison of  $\Delta XAFS$  with the theoretical Pt–H EXAFS function (calculated with the FEFF7 XAFS code assuming a Pt–H distance of 1.8 Å) indicated that  $\Delta XAFS$  is dominated by Pt–H scattering [31]. Because scattering is primarily resonant and hydrogen has only low binding 1s electrons, the hydrogen backscattering cross section is only significant at low photoelectron kinetic energies. In the normal EXAFS analysis, the Fourier transform of  $\chi$  is typically taken from  $k = 3$  to  $14 \text{ \AA}^{-1}$ . At these photoelectron energies there is almost no scattering from the H atoms.

Subtraction of the  $L_{II}$  from the  $L_{III}$  edge (without chemisorbed hydrogen) gives the electronic contributions to the near edge due to changes in the occupancy of the valence band:  $L_{III}(Pt) - L_{II}(Pt) = \Delta VB$ . The changes in the valence band for the Pt/LTL catalysts are shown in Fig. 5. Despite the large difference in their catalytic and spectroscopic properties, comparison of the valence band spectra indicates that there is little difference between the catalysts. In addition, these small changes are not systematic and do not correlate with the composition of the support, TOF or infrared spectra.

The AS can be isolated by a double subtraction of the  $L_{III}$  and the  $L_{II}$  edges with and without chemisorbed hydrogen [31]:  $[L_{III}(H_2-Pt) - L_{III}(Pt)] - [L_{II}(H_2-Pt) - L_{II}(Pt)] = [L_{III} - L_{II}](H_2-Pt) - [L_{III} -$

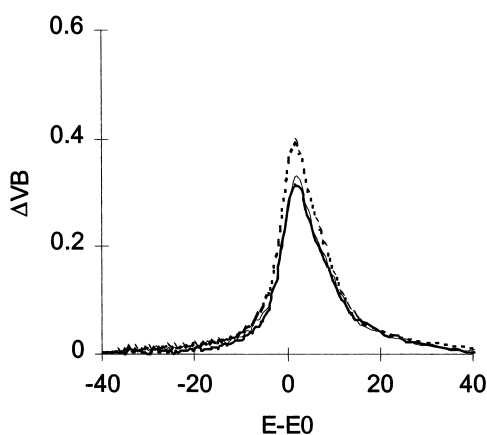


Fig. 5.  $L_{III}(Pt) - L_{II}(Pt) = \Delta VB$ ; (thin solid) Pt/LTL (0.63); (dotted) Pt/LTL (0.96); (bold solid) Pt/LTL (1.25).

$L_{II}(Pt) = AS$ . The contribution to the near-edge spectra from the AS is shown in Fig. 6 (solid line). From the spectra, it is apparent that the features of the shape resonance are highly dependent on composition of the support.

The shape resonance spectra in Fig. 6 were fit with the Fano expression given above. Since  $\Phi$  and  $\Gamma$  are strongly interdependent and the width is uncertain because of the experimental broadening,  $\Gamma$  and  $E_{res}$  are coupled utilizing the relation  $\Phi = \alpha + \beta E_{res}$ . The resonant line shapes were then fit with a total of 11 parameters, i.e.,  $E_{res}$ ,  $\Gamma$ , and  $A$  for each resonance plus  $\alpha$  and  $\beta$ . The theoretical fit (dotted line in Fig. 6) was broadened by 5 eV to account for experimental and lifetime broadening (the experimental resolution is around 3 eV and the core hole width is around 5 eV). The optimum non-linear, least-square fits are given in Table 4. The dramatic reversal in line shape of the Pt–H antibonding orbital for the different catalysts is reproduced by the Fano expression.

The difference in energy between the antibonding orbital and the Fermi level,  $E_{res}$ , systematically decreases from plus to minus as the composition of the LTL support changes from acidic to neutral to alkaline. The negative resonance energy for the alkaline catalyst with respect to the edge may, in part, be caused by the initial choice of  $E_0$  at 0.6 times the step height of the  $L_2$  Pt spectrum since  $E_0$  may not be at the actual Fermi level of the cluster. More importantly, however, the negative  $E_{res}$  likely results

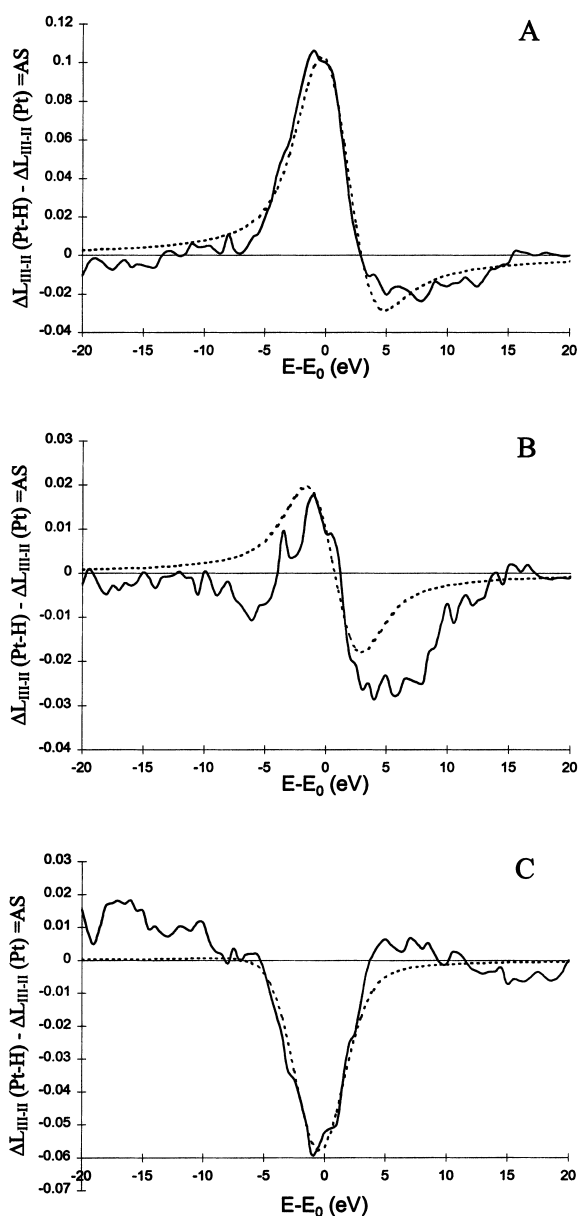


Fig. 6. Shape resonance (solid line),  $\Delta L_{III-II}(H_2-Pt) - \Delta L_{III-II}(Pt)$  and model fit (dotted line) of the Fano line shape with fit parameters from Table 4. (A) Pt/LTL (0.63); (B) Pt/LTL (0.96); (C) Pt/LTL (1.25).

because the resonance (localized primarily on the Pt atom with the core hole) is pulled down below the Fermi level by the core hole–electron attraction. Consistent with the final-state rule, the values of  $E_{res}$  do

Table 4  
Fitting parameters for shape resonance<sup>a</sup>

Catalyst	$A$ ( $\pm 0.03$ )	$E_{\text{res}}$ (eV) ( $\pm 0.3$ )	Width, $\Gamma$ (eV) ( $\pm 0.4$ )	$\Phi$ (calculated) ( $\pm 0.1$ )
Pt/LTL (0.63)	0.15	2.0	2.1	0.47
Pt/LTL (0.96)	0.04	1.1	3.4	0.10
Pt/LTL (1.25)	0.08	-1.2	1.2	-0.76

<sup>a</sup>  $\Phi = \alpha + \beta E_{\text{res}}$  with optimal  $\alpha = -0.3 \pm 0.1$  and  $\beta = 0.38 \pm 0.03$ .

not reflect the actual energy of the AS in the ground state but in the presence of a core hole.

From electron scattering theory, the natural width of the resonance ( $\Gamma$ ) is determined by the magnitude of the quantum mechanical matrix element,  $V$ , involving the Pt valence band and the Pt–H AS, i.e.,  $\Gamma = 2\pi V^2$ . Table 4 shows that the width of the resonance initially increases as  $E_{\text{res}}$  decreases. This occurs because the increasing degeneracy of the resonance with the Pt VB increases  $V$  and enables faster auto-ionization of the resonant electron. However, the resonance width dramatically decreases when the AS drops below the Fermi level since now the electron cannot escape into the degenerate, filled Pt orbitals.

The background phase parameter,  $\Phi$ , is assumed to be proportional to  $E_{\text{res}}$  in the expression  $\alpha + \beta E_{\text{res}}$ . Here  $\beta$  includes the entire energy dependence of the total background phase,  $2kR + 2\delta_a + \delta_s$  (the latter indicating the phase of the absorber and the scatterer). FEFF7 calculations for Pt–H scattering shows that indeed  $\Phi$  varies linearly with energy at lower energies, giving the phase  $\Phi = -0.5 + 0.37E_{\text{res}}$  for a Pt–H distance of 1.8 Å. The optimal fit to the AS line shapes, gives  $\beta = 0.38 \pm 0.03$  in excellent agreement with the FEFF7 results. The optimum  $\alpha$  parameter of  $-0.3 \pm 0.1$  is in reasonable agreement compared to  $-0.5$  obtain with FEFF7 since  $\alpha$  depends on the inner potential  $E_0$ , which is not accurately predicted by the FEFF7 code.

#### 4. Discussion

Metal–support interactions are well known to affect the activity of Pt and Pd catalysts for benzene hydrogenation [7,8,44,45], and propane [43] and neopentane hydrogenolysis [1,5,9–11,46]. Several studies have demonstrated that the TOF is higher on acidic supports [1–11,43–46] and decreases on alka-

line supports [9–11]. In addition, shifts in the infrared spectra of adsorbed CO are generally interpreted as changes in electronic properties of the catalytically active surface atoms [22,23]. Theoretical calculations and experimental studies have shown that the linear to bridging ratio of adsorbed CO is also a good indicator of changes in the electronic properties of the metal [38]. Fig. 7 shows that there is an increase in the ln(TOF) for the Pt/LTL catalysts with increasing linear to bridging ratio. This correlation suggests that the changes, which affect the infrared spectra, also influence the catalytic properties. Thus, the change in TOF is due to an electronic change in the Pt particles induced by the metal–support interaction.

Several electronic models for the metal–support interaction have been proposed. Based on infrared and X-ray photoelectron spectroscopy, two models suggest that the changes in TOF result from a transfer of electron density between the metal and the support, where, e.g., on acidic supports the increase in TOF is thought to be due to electron deficient metal particles [1]. Because the catalytic and spectroscopic properties are widely associated with support acidity, one model proposes that hydrogen ions are delocalized over the metal surface, transferring metal electron density to the proton adduct [5,6]. An alternative model suggests that the electronic properties of the metal particles interact with the support oxide ions [4,9,11]. The magnitude and direction of change in the catalytic properties are determined by the charge on the oxide ion [4].

If the electron transfer models were correct, the intensity of the valence band in the near-edge spectra would decrease in the order Pt/LTL(0.63) > Pt/LTL(0.93) > Pt/LTL(1.25). However, the differences in the valence band spectra are small and do not correlate with the TOF or the infrared spectra. For example, the VB spectra of Pt/LTL (0.63) and Pt/LTL (1.25) are nearly identical suggesting there is little difference in the number of valence electrons. The

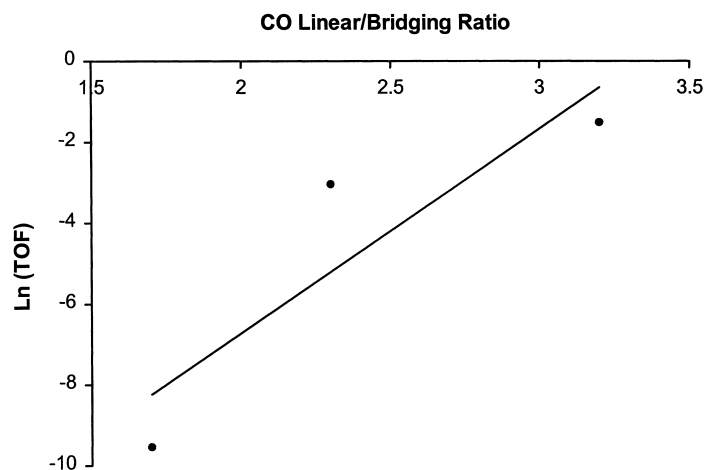


Fig. 7. Relationship between the  $\ln(\text{TOF})$  and the infrared linear to bridging ratio of adsorbed CO.

change in catalytic activity and spectroscopic properties therefore do not appear to result from a transfer of electron density between the metal and support.

Based on theoretical calculations, a polarization model has also been proposed to account for the metal–support interaction [25,26]. The model suggests that highly charged cations of the support attract electrons of nearby metal atoms. As a result, the electron density of the atoms near the support surface increases while the atoms on the opposite side of the cluster are electron deficient. In this model, there is no net change in electron density for the cluster; however, polarization of the electron density leaves those atoms, which participate in the catalysis electron deficient. While this model is consistent with the catalysis, IR and valence band spectra, this model is not consistent with the EXAFS structural determination. The results of this and previous EXAFS structural studies indicate that the Pt particles are in direct contact with the support oxide and there is no evidence that cation or (support) metal ions interact with the Pt atoms. We conclude, therefore, that the polarization model is incorrect.

#### 4.1. A new model for the metal–support interaction

While the results of the valence band spectra indicate little difference between the Pt/LTL catalysts, the shape resonance of the Pt–H antibonding

orbital is strongly influenced by the acidic or alkaline properties of the support [31]. Comparison of the fitting parameters in Table 4 indicates that there is a systematic decrease in  $E_{\text{res}}$  in the order Pt/LTL(0.63) > Pt/LTL(0.93) > Pt/LTL(1.25).  $E_{\text{res}}$  is the difference in energy between the Fermi level and the antibonding orbital.

The energy of the H 1s orbital is lower than the energy of the Pt valence orbitals. Since the energy of the H 1s bonding orbital does not change with catalyst composition, we conclude that change in  $E_{\text{res}}$  results from a shift in the energy of the Pt valence orbitals due to the interaction with the support. The more similar the energy of the Pt and H orbitals, the stronger is the bond and the greater is the difference in energy between the Pt–H antibonding orbital and the Fermi level, i.e., there is a larger  $E_{\text{res}}$  (see Fig. 8). The largest  $E_{\text{res}}$  of Pt/LTL (0.63) indicates the strongest overlap of the bonding orbitals and a shift to higher binding energy of the Pt valence orbitals. The implication from the shape resonance analysis is that the support alters the energy of the Pt orbitals at the Fermi level affecting the chemisorption energies of adsorbates. The electronic basis of this model does not depend on the transfer of electron density between the metal particle and the support, but a shift in the Pt 5d valence band.

Based on the EXAFS results, we also conclude that the shifts in the energy of the valence orbitals result from an interaction of the metal with the support oxide

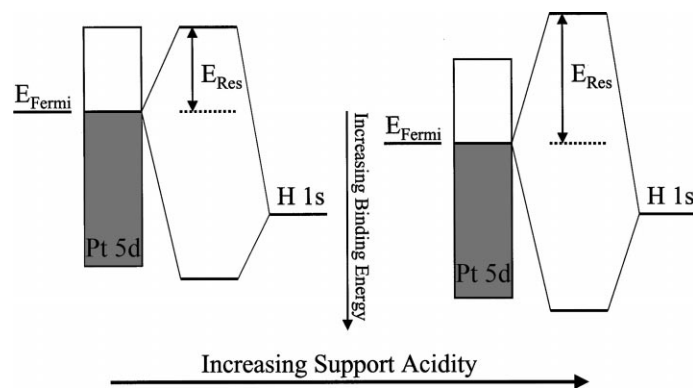


Fig. 8. Molecular orbital diagram of the bonding and antibonding orbitals for the Pt valence and the H 1s orbitals with changing support composition.

ions. While the metal–support interaction is generally described in terms of the support acidity or alkalinity, it is more correct to describe the interaction in terms of the charge on the oxide ions. The higher the negative charge on the oxygen, the smaller is the decrease in energy (lower binding energy) of the Pt valence orbitals [47].

Several studies have shown that exchange of NaY by  $\text{La}^{3+}$  or  $\text{H}^+$  ions results in an increase in the O, Si and Al XPS binding energies [48–50]. Recently, a theoretical study presented evidence that the origin of these shifts are due to changes in Madelung potential, rather than to a change in charge transfer between the ions of the zeolite lattice [50]. The consequence of the Madelung potential model is that the influence of  $\text{H}^+$ ,  $\text{La}^{3+}$  and  $\text{Na}^+$  ions are similar in origin. Generally, the support composition determines the Madelung potential and the surface potential interacts with the metal particles influencing the energy of their valence orbitals. While the energy of the 5d valence band increases to higher binding energy with increasing support acidity, the number of 5d and 6s valence electrons does not change appreciably. Although all ions of the support contribute to the surface potential, because the metal atoms are in contact with the oxide surface, the atomic potential of the oxide ions has the largest effect on the energy of the valence orbitals.

While the new model of the metal–support interaction correlates with the TOF and is consistent with the analysis of the shape resonance and valence band of the near-edge absorption spectra, it is also consis-

tent with the IR and XPS spectroscopies. For example, the Pd XPS binding energies in Pd/LTL catalysts decreases as the composition of the support changes from acidic to neutral to alkaline [9]. The Madelung potential model suggests that the energy of the valence orbitals decreases in the same order. The lower energy of the Pd Fermi level on alkaline support would result in a lower binding energy as observed. Similarly, the new model is consistent with IR spectroscopy of adsorbed CO: there is a shift to lower frequency and a decrease in the linear to bridging ratio as the alkalinity of the support increases. For CO, the energy of the  $\pi^*$  orbitals is above the Pt Fermi level energy. A decrease in the binding energy of the Pt valence orbitals would result in a better overlap of the  $d-\pi^*$  orbitals, this leading to more  $\pi^*$  electron density, a weaker C–O bond and a shift in the IR bands to lower energy. Likewise, the theoretical calculations predict a shift from linear to bridge-bonded CO when there is a better overlap of the  $d-\pi^*$  orbitals.

In summary, we propose a new model for the metal–support interaction where a Coulombic interaction between the interatomic surface potential and the metal atomic potential results in a shift in the energy of the valence orbitals at the Fermi level [47]. As the electron density of the support oxide decreases or becomes more acidic, the binding energy of the metal valence orbitals increases. The shift in the energy of the Fermi level affects the chemisorption energies of adsorbates and is consistent with the known catalytic and spectroscopic properties.

Table 5  
Neopentane TOF for Pt on amorphous supports

1.5% Pt catalyst	TOF <sup>a</sup>
SiO <sub>2</sub> –Al <sub>2</sub> O <sub>3</sub>	$2.7 \times 10^{-2}$
ZrO <sub>2</sub>	$1.4 \times 10^{-2}$
Al <sub>2</sub> O <sub>3</sub>	$5.6 \times 10^{-3}$
SiO <sub>2</sub>	$2.4 \times 10^{-3}$
CeO <sub>2</sub>	$2.2 \times 10^{-3}$
K–Al <sub>2</sub> O <sub>3</sub> (0.25 wt.% K)	$1.5 \times 10^{-3}$
K–Al <sub>2</sub> O <sub>3</sub> (0.75 wt.% K)	$2.5 \times 10^{-4}$
MgO–Al <sub>2</sub> O <sub>3</sub>	$5.3 \times 10^{-5}$

<sup>a</sup> Determined at 325°C.

#### 4.2. Implications for catalyst development

A complete discussion of all the issues of catalyst development are beyond the scope of the current paper. However, a few examples of how the metal–support interaction can be used to modify the performance of catalysts will be given. While this and many previous studies have shown that the degree of ion exchange can affect the TOF of metals in zeolites, the effect is not limited to the number of protons and alkali content on zeolite supports. Table 5 gives the Pt TOF for neopentane hydrogenolysis for a number of amorphous supports. For most supports, the Pt dispersion was nearly constant at 0.6. As with zeolites, the TOF increases by about 500 times and, generally, parallels the acidic/basic properties of the support. For example, the Pt TOF decreases in the order silica–alumina > alumina > magnesia–alumina. Pt on zirconium oxide also has a very high TOF and is often observed to give high activity for supported metal

catalysts. Also shown in Table 5, the TOF decreases by a factor of about 20 with increasing amounts of alkali in the order alumina > alumina(0.25 wt.% K) > alumina(0.75 wt.% K). This latter effect is more properly described as a promoter effect, rather than a true support effect, i.e., the catalytic activity of Pt is modified by a small addition of a non-catalytic component.

Promoter effects, however, are not limited to the alkali elements. Table 6 shows the effect of several promoters for Pt on silica and alumina. For Pt/silica, as observed with alumina, the TOF decreases with increasing amounts of alkali. Addition of aluminum, however, leads to an increase in TOF. For these catalysts, the shifts in the IR frequency of adsorbed CO, the changes in the linear/bridging ratio and the correlation with the TOF are similar to those of the Pt/LTL catalysts above [11,47]. The results for the Pt/alumina catalysts show that, in addition to alkali metals, alkaline earth and rare earth oxides also modify the activity of Pt. The magnitude of the effect is consistent with the proposed Madelung potential model. At an equivalent number of moles of promoter, the largest effect is observed for alkali ions, which are most basic, while the decrease in TOF for lanthanum oxide is comparatively small. The higher the negative charge on the oxide, the greater the shift in the energy of the Pt valence orbitals and the larger the change in the TOF. Each of the above series of catalysts is currently under more extensive characterization.

While support and promoter effects on the TOF are important, Pt on acidic supports is also more sulfur tolerant than Pt on neutral and alkaline supports [12–20]. Ion exchange of Pt into acidic zeolites, rather than

Table 6  
Elemental analysis, dispersion and neopentane TOF for Pt/SiO<sub>2</sub> and Pt/Al<sub>2</sub>O<sub>3</sub>

1.5% Pt catalyst	Al (wt.%)	M (wt.%)	K (wt.%)	TOF <sup>a</sup>	TOF <sup>b</sup>
SiO <sub>2</sub> –Al (0.10)	0.10	–	–	$3.1 \times 10^{-2}$	–
SiO <sub>2</sub>	–	–	–	$5.5 \times 10^{-3}$	–
SiO <sub>2</sub> –K (0.39)	–	–	0.39	$4.5 \times 10^{-4}$	–
SiO <sub>2</sub> –K (0.77)	–	–	0.77	$2.2 \times 10^{-4}$	–
SiO <sub>2</sub> –K (1.14)	–	–	1.14	$8.0 \times 10^{-5}$	–
Al <sub>2</sub> O <sub>3</sub>	–	–	–	–	$6.4 \times 10^{-3}$
Cs–Al <sub>2</sub> O <sub>3</sub>	–	2.9	–	–	$0.6 \times 10^{-3}$
Sr–Al <sub>2</sub> O <sub>3</sub>	–	3.2	–	–	$3.5 \times 10^{-3}$
La–Al <sub>2</sub> O <sub>3</sub>	–	3.6	–	–	$5.3 \times 10^{-3}$

<sup>a</sup> Determined at 390°C.

<sup>b</sup> Determined at 350°C.

supported on the alumina matrix, has in recent years resulted in more sulfur tolerant paraffin isomerization catalysts [12]. Similarly, exchange of Pt and Pd into Y zeolite has led to development of noble metal catalysts for saturation of aromatic distillate fuels, which contain high levels of sulfur [51–54].

In a previous study of sulfur tolerance of Pt/LTL catalysts, it was shown that upon exposure to H<sub>2</sub>S, the surfaces of both acidic and alkaline catalysts were nearly saturated by Pt–S bonds resulting in large decreases in the initial activities (per gram), although the TOFs were nearly unchanged [20]. For Pt on acidic supports, however, the S to Pt ratios were lower. As a result, the rate of deactivation due to coke formation was lower than that for Pt on alkaline supports. The increased sulfur tolerance of acidic-supported noble metal catalysts appears to result primarily from the higher intrinsic TOF, and its resistance to coke deactivation due to the lower surface coverage of sulfur.

Although acidic-supported metal catalysts are more sulfur tolerant, for many processes acid-catalyzed reactions are undesirable, leading to yield loss and deactivation. Development of non-acidic sulfur tolerant metal catalysts, therefore, is highly desirable for these applications. If the metal–support interaction determines the catalytic properties, the sulfur tolerance will parallel the TOF. Recently it was shown that in the absence of support acidity, exchange of NaY by polyvalent cations results in an increase in the TOF similar to that in HY [55]. We are investigating the potential for development of sulfur resistant catalysts which contain no acid sites. In the future, it is expected that catalysts which are highly resistant to sulfur poisoning can be developed by optimization of the metal–support interaction.

## 5. Conclusions

The TOFs of noble metal catalysts are strongly dependent on the composition of the support and the presence of non-catalytic promoters, and the activities decrease in the order acidic > neutral > alkaline. In addition, the correlation of ln(TOF) with the linear to bridging ratio of adsorbed CO in the infrared spectra indicates that these changes are due to a modification of the electronic properties in the metal particles. From EXAFS spectroscopy, the Pt atoms interact

with the oxygen ions of the support, while there is no interaction with the Al, Si and K ions. The electronic and geometric contributions to the near-edge X-ray absorption spectra can be isolated by subtraction of the L<sub>III</sub> and L<sub>II</sub> edges with and without hydrogen, and suggest that the number of electrons in the valence band is unchanged by the support interaction. In addition, at the L<sub>III</sub> near-edge spectra, the resonance energy, which is the difference in energy between the Fermi level and the Pt–H antibonding orbital, is strongly dependent on the composition of the support and decreases in the order acidic > neutral > alkaline. Based on the above characterizations, a new electronic model for the metal–support interaction is proposed where the energy of the metal valence orbitals shifts due to the interaction with the Madelung potential of the support. Shifts in the energy of the Fermi level affects the chemisorption energy of adsorbates and is responsible for changes in the TOF. The metal–support interaction is widely applicable to many metals and supports and can be used to optimize the performance of the catalysts.

## References

- [1] R.A. Della Betta, M. Boudart, in: J.W. Hightower (Ed.), Proceedings of the Fifth International Congress on Catalysis, Vol. 2, North-Holland, Amsterdam, 1973, p. 1329.
- [2] G. Larsen, G.L. Haller, Catal. Lett. 3 (1989) 103.
- [3] A.P.J. Jansen, R. van Santen, J. Phys. Chem. 94 (1990) 6764.
- [4] A. de Mallmann, D. Marthomeuf, J. Chim. Phys. 87 (1990) 535.
- [5] S.T. Homeyer, Z. Karpinski, W.M.H. Sachtler, J. Catal. 123 (1990) 60.
- [6] W.M.H. Sachtler, A.Y. Stakheev, Catal. Today 12 (1992) 283.
- [7] D.L. Shawn, M.A. Vannice, J. Catal. 143 (1993) 539.
- [8] D.L. Shawn, M.A. Vannice, J. Catal. 143 (1993) 554.
- [9] B.L. Mojet, M.J. Kappers, J.C. Muijsers, J.W. Niemantsverdriet, J.T. Miller, F.S. Modica, D.C. Koningsberger, in: J. Weitkamp, H.G. Karge, H. Pfeifer, W. Hölderich (Eds.), Studies in Surface Science and Catalysis, Zeolites and Related Microporous Materials: State of the Art 1994, Vol. 84B, Elsevier, Amsterdam, 1994, p. 909.
- [10] F.S. Modica, J.T. Miller, B.L. Meyers, D.C. Koningsberger, Catal. Today 21 (1994) 37.
- [11] B.L. Mojet, M.J. Kappers, J.T. Miller, D.C. Koningsberger, in: J.W. Hightower, W.N. Delgass, E. Iglesia, A.T. Bell (Eds.), Studies in Surface Science and Catalysis, Eleventh International Congress on Catalysis, Vol. 101B, Elsevier, Amsterdam, 1996, p. 1165.
- [12] J.A. Rabo, V. Shomaker, P.E. Pickert, in: W.M.H. Sachtler, G.C.A. Schuit, P. Zwietering (Eds.), Proceedings of the Third

- International Congress on Catalysis, Vol. 2, North-Holland, Amsterdam, 1965, p. 1264.
- [13] G.D. Chukin, M.V. Landau, V.Y. Kruglikov, D.A. Agievskii, B.V. Smirnov, A.L. Belozarov, V.D. Asrieva, N.V. Goncharova, E.D. Radchenko, O.D. Konoval'chikov, A.V. Agafonov, in: G.C. Bond, P.B. Wells, F.C. Tompkins (Eds.), Proceedings of the Sixth International Congress on Catalysis, Chemical Society, London, 1977, p. 668.
- [14] M.V. Landau, V.Y. Kruglikov, N.V. Goncharova, O.D. Konoval'chikov, G.D. Chukin, B.V. Smirnov, V.I. Malevich, Kinet. Catal. 17 (1976) 1104.
- [15] S.M. Kovach, R.A. Kmecak, Am. Chem. Soc., Pre. Div. Petr. Chem. Houston 25 (1) (1980) 79.
- [16] R. Frety, P.N. Da Silva, M. Guenin, Catal. Lett. 3 (1989) 9.
- [17] R. Frety, P.N. Da Silva, M. Guenin, Appl. Catal. 57 (1990) 99.
- [18] L.J. Hoyos, M. Primet, H. Praliaud, J. Chem. Soc., Faraday Trans. 88 (1992) 113.
- [19] P. Marecot, J.R. Mahoungou, J. Barbier, Appl. Catal. A 101 (1993) 143.
- [20] J.T. Miller, D.C. Koningsberger, J. Catal. 162 (1996) 209.
- [21] P. Gallezot, Catal. Rev.-Sci. Eng. 20 (1979) 121.
- [22] P. Gallezot, J. Datka, J. Massardier, M. Primet, B. Imelik, in: G.C. Bond, P.B. Wells, F.C. Tompkins (Eds.), Proceedings of the Sixth International Congress on Catalysis, Vol. 2, 1977, p. 696.
- [23] C. Naccache, M. Primet, M.V. Mathieu, Adv. Chem. Ser. 121 (1973) 66.
- [24] A.Yu. Stakheev, W.M.H. Sachtler, J. Chem. Soc., Faraday Trans. 87 (1991) 3703.
- [25] A.P.J. Jansen, R.A. van Santen, J. Phys. Chem. 94 (1990) 6764.
- [26] E. Sanchez-Marcos, A.P.J. Jansen, R.A. van Santen, Chem. Phys. Lett. 167 (1990) 399.
- [27] J.W. Cook Jr., D.E. Sayers, J. Appl. Phys. 52 (1981) 5024.
- [28] M. Vaarkamp, J.C. Linders, D.C. Koningsberger, Physica B 208–209 (1995) 159.
- [29] B.L. Mojet, M.S. Hoogenraad, A.J. van Dillen, J.W. Geus, D.C. Koningsberger, J. Chem. Soc., Faraday Trans. 93 (24) (1997) 4371.
- [30] D.C. Koningsberger, in: J. Baruchel, J.L. Hodeau, M.S. Lehmann, J.R. Regnard, C. Schlenker (Eds.), Applications to Solid State Physics and Chemistry, Neutron and Synchrotron Radiation for Condensed Matter Studies, Vol. II, Springer, Berlin, 1994, p. 213.
- [31] D.E. Ramaker, B.L. Mojet, M.T. Garriga Oostenbrink, J.T. Miller, D.C. Koningsberger, Phys. Chem. Chem. Phys. 1 (1999) 2293.
- [32] L.F. Mattheiss, R.E. Dietz, Phys. Rev. B 22 (4) (1980) 1663.
- [33] B. Hammer, J.K. Nørskov, Nature 376 (1995) 238.
- [34] J.R. Taylor, Scattering Theory: The Quantum Theory of Nonrelativistic Collisions, E. Krieger Publ. Comp., Florida, 1983, p. 243.
- [35] N.A. Bhore, M.T. Klein, K.B. Bischoff, Ind. Eng. Chem. Res. 29 (1990) 313.
- [36] R. van Hardeveld, F. Hartog, Adv. Catal. 22 (1972) 75.
- [37] F. Stoop, F.J.C.M. Toolenaar, V. Ponec, J. Catal. 73 (1982) 50.
- [38] R.A. van Santen, J. Chem. Soc., Faraday Trans. I 83 (1987) 1915.
- [39] B.L. Mojet, J.T. Miller, D.C. Koningsberger, J. Phys. Chem. 103 (1999) 2724.
- [40] F.W. Lytle, R.B. Greegor, E.C. Marques, V.A. Biebesheimer, D.R. Sandstrom, G.H. Horsley, G.H. Via, J.H. Sinfelt, J. ACS Symp. Ser. 288 (1985) 280.
- [41] M.G. Samant, M. Boudart, J. Phys. Chem. 95 (1991) 4070.
- [42] M. Vaarkamp, J.T. Miller, F.S. Modica, D.C. Koningsberger, Jpn. J. Appl. Phys. 32 (1993) 460.
- [43] M. Vaarkamp, J.T. Miller, F.S. Modica, G.S. Lane, D.C. Koningsberger, in: L. Guzzi, F. Solmosi, P. Tetenyi (Eds.), Studies in Surface Science and Catalysis, Proceedings of the 10th International Congress on Catalysis, Vol. 75A, Budapest 1992, Elsevier, Amsterdam, 1993, p. 809.
- [44] F. Figueras, R. Gomez, M. Primet, Adv. Chem. Ser. 121 (1973) 480.
- [45] S.D. Lin, M.A. Vannice, J. Catal. 143 (1993) 539.
- [46] Z. Karpinski, S.N. Gandhi, W.M.H. Sachtler, J. Catal. 141 (1993) 337.
- [47] B.L. Mojet, J.T. Miller, D.E. Ramaker, D.C. Koningsberger, J. Catal. 186 (1999) 373.
- [48] Y. Okamoto, M. Ogawa, A. Maezawa, T. Imanaka, J. Catal. 112 (1988) 427.
- [49] J. Stoch, J. Lercher, S. Ceckeiewicz, Zeolites 12 (1992) 82.
- [50] W. Grunert, M. Muhler, K.-P. Schroder, J. Sauer, J. Phys. Chem. 98 (1994) 10920.
- [51] J.K. Minderhoud, J.P. Lucien, A process for hydrogenation of hydrocarbon oils, European Patent 303,332.
- [52] S.G. Kukes, F.T. Clark, P.D. Hopkins, Distillate hydrogenation, US Patent 5,147,426.
- [53] S.G. Kukes, F.T. Clark, P.D. Hopkins, L.M. Green, Distillate hydrogenation, US Patent 5,151,172.
- [54] J.P. van den Berg, J.P. Lucien, G. Germaine, G.L.B. Thielemans, Fuel Proc. Technol. 35 (1993) 119.
- [55] D.C. Koningsberger, J. de Graaf, B.L. Mojet, D.E. Ramaker, J.T. Miller, Appl. Catal. A: Gen. 191 (2000) 205.